

The SLUGGS Survey: stellar masses and effective radii of early-type galaxies from Spitzer Space Telescope 3.6 μ m imaging

Duncan A. Forbes^{1*}, Luciana Sinpetru², Giulia Savorgnan¹, Aaron J. Romanowsky^{3,4}, Christopher Usher⁵ and Jean Brodie⁴

¹Centre for Astrophysics & Supercomputing, Swinburne University, Hawthorn VIC 3122, Australia

²Institute for Astronomy, University of Edinburgh, Royal Observatory, Blackford Hill, Edinburgh EH9 3HJ, UK

³Department of Physics and Astronomy, San José State University, One Washington Square, San Jose, CA 95192, USA

⁴University of California Observatories, 1156 High Street, Santa Cruz, CA 95064, USA

⁵Astrophysics Research Institute, Liverpool John Moores University, 146 Brownlow Hill, Liverpool L3 5RF, UK

4 October 2018

ABSTRACT

Galaxy starlight at 3.6 μ m is an excellent tracer of stellar mass. Here we use the latest 3.6 μ m imaging from the Spitzer Space Telescope to measure the total stellar mass and effective radii in a homogeneous way for a sample of galaxies from the SLUGGS survey. These galaxies are representative of nearby early-type galaxies in the stellar mass range of $10 < \log M_*/M_\odot < 11.7$, and our methodology can be applied to other samples of early-type galaxies. We model each galaxy in 2D and estimate its total asymptotic magnitude from a 1D curve-of-growth. Magnitudes are converted into stellar masses using a 3.6 μ m mass-to-light ratio from the latest stellar population models of Röck et al., assuming a Kroupa IMF. We apply a ratio based on each galaxy’s mean mass-weighted stellar age within one effective radius (the mass-to-light ratio is insensitive to galaxy metallicity for the generally old stellar ages and high metallicities found in massive early-type galaxies). Our 3.6 μ m stellar masses agree well with masses derived from 2.2 μ m data. From the 1D surface brightness profile we fit a single Sersic law, excluding the very central regions. We measure the effective radius, Sersic n parameter and effective surface brightness for each galaxy. We find that galaxy sizes derived from shallow optical imaging and the 2MASS survey tend to underestimate the true size of the largest, most massive galaxies in our sample. We adopt the 3.6 μ m stellar masses and effective radii for the SLUGGS survey galaxies.

Key words: galaxies: masses – galaxies: evolution – galaxies: individual

1 INTRODUCTION

The total stellar mass is a fundamental parameter for any galaxy. Not only do many other galaxy properties vary with stellar mass, but an accurate measure of stellar mass is required to probe the dark matter content (i.e. the total mass minus the stellar mass) in a galaxy. However, measuring the total stellar mass is problematic, even once the total luminosity has been accurately measured. For example, a common approach is to measure the total luminosity of a galaxy at near-IR wavelengths for which the light mostly comes from old stars that dominate the mass, and the effects of dust are much reduced compared to optical wavelengths. A typical approach is to use the full-sky ground-based near-IR imaging of the 2MASS survey (Jarrett et al. 2003). However it has been reported that the 2MASS reduction pipeline systematically underestimates the total

luminosity and size of large, nearby galaxies due to a truncation of their surface brightness profiles (Schombert & Smith 2012; Scott et al. 2013).

An alternative approach is to use the 3.6 μ m band of the Spitzer Space Telescope (Werner et al. 2004) or the 3.4 μ m band of the WISE space telescope (Wright et al. 2010). Such wavelengths are particularly well suited to measure the stellar masses of galaxies. For example, Norris et al. (2014) concluded that photometry from WISE can “...provide extremely simple, yet robust stellar mass tracers for dust free older stellar populations...”. This is because the 3.4–3.6 μ m light from galaxies is dominated by the light from old stars, and it is less effected by variations in the star formation history than shorter wavelengths. Although intermediate-aged stars, hot dust and polycyclic aromatic hydrocarbons may contribute to the emission at 3.6 μ m, these sources are negligible for most early-type galaxies which are dominated by old stellar populations (Meidt et al. 2012; Querejeta et al. 2015).

* E-mail: dforbes@swin.edu.au

Here we use $3.6\mu\text{m}$ imaging from the Spitzer Space Telescope. The $3.6\mu\text{m}$ mass-to-light ratio ($M/L_{3.6}$) has virtually no dependence on metallicity, and only a very small dependence on age for old stellar ages. We use the latest single-burst stellar population models (Röck et al. 2015) which are based on empirical mid-infrared stellar spectra (Cushing et al. 2005; Rayner et al. 2009). These models cover a range of metallicity, ages and IMF slopes. They are shown to reproduce well the mid-infrared colours of early-type galaxies. For a Kroupa IMF, these models give $M/L_{3.6} \sim 0.8$ for a stellar population mean age of 9 Gyr, with a variation between different isochrones, i.e. from BaSTI and Padova, of ~ 0.05 . For a metallicity range of $[\text{Fe}/\text{H}] = -0.4$ to solar (i.e. typical of the mean values for massive early-type galaxies), the variation is insignificant at ~ 0.02 . We note that the Flexible Stellar Population Synthesis (FSPS; Conroy & Gunn 2010) models with AGB circumstellar dust included (Villaume et al. 2015) also give $M/L_{3.6} \sim 0.8$ for a 9 Gyr old, moderately metal-rich population. Meidt et al. (2014) adopted a constant value of $M/L_{3.6} = 0.6$ for their S4G sample, although their sample was dominated by late-type galaxies with younger mean ages on average.

Stellar mass-to-light ratios have a strong dependence on the Initial Mass Function (IMF). The $M/L_{3.6}$ values quoted above refer to a Kroupa IMF. Salpeter and other IMFs tend to have higher $M/L_{3.6}$ values by a factor of ~ 1.5 -3 (Röck et al. 2015), which would lead to larger stellar masses for a given $3.6\mu\text{m}$ luminosity. Recent work indicates that the IMF for early-type galaxies is skewed to low mass stars (see e.g. Ferre-Mateu et al. 2013; Martin-Navarro et al. 2015; McConnell et al. 2016). Currently, it is not yet clear what is causing the IMF variations nor whether these variations are confined to galaxy central regions, high metallicity regions or spheroids. Here we adopt a Kroupa IMF for our global $M/L_{3.6}$ but caution that the stellar masses for massive elliptical galaxies may need revising upwards.

Since $M/L_{3.6}$ varies with stellar age, an age-appropriate ratio should be employed. Here we adopt an age dependent mass-to-light ratio from the Röck et al. (2015) models using mean stellar ages from the literature. We assume a Kroupa IMF.

The SLUGGS survey targets 25 nearby massive early-type galaxies in different environments and 3 so-called bonus galaxies (Brodie et al. 2014). We study the kinematics and metallicity of both the galaxy itself, and its system of globular clusters, to large galactocentric radii. The sample galaxies are chosen to cover a range of key parameters including stellar mass and physical size. Until now, the approach in the SLUGGS survey to measure stellar mass has been to obtain the extinction-corrected K-band ($2.2\mu\text{m}$) magnitude from the 2MASS extended galaxy catalog and apply the correction of Scott et al. (2013) for missing light. We then applied a constant $M/L_{2.2} = 1$ irrespective of stellar metallicity or age. A value of unity is simplistic, but a reasonable approximation for a very old stellar population with a Kroupa IMF (Bruzual & Charlot 2003).

The effective radii (R_e) of the SLUGGS galaxies are listed in Brodie et al. (2014, B14), which are based on Cappellari et al. (2011). Cappellari et al. used sizes from both optical and near-IR imaging. They noted that the near-IR sizes from the 2MASS survey (Jarrett et al. 2003) for the largest, most massive galaxies appear to be systematically underestimated and they scaled-up their near-IR sizes to match the optical sizes on average. A recent study by van den Bosch (2016) also found the 2MASS survey to underestimate the sizes (and total fluxes) of nearby galaxies. Accurate galaxy effective radii are important in order to compare galaxies on a similar relative scale. For example the SLUGGS survey and other

integral field spectroscopy studies, derive kinematic profiles as a function of effective radii and measure properties such as specific angular momentum within $1 R_e$ (Arnold et al. 2014; Alabi et al. 2015; Foster et al. 2016). Thus the photometric effective radii need to be accurate in order to correctly compare kinematic properties between different galaxies. Effective radii, combined with accurate stellar masses, are needed to probe the dark matter fraction within a given multiple of R_e . The Spitzer Space Telescope imaging presented here offers an opportunity to revisit the sizes and masses of the SLUGGS early-type galaxies.

In the next sections we present the $3.6\mu\text{m}$ data from the Spitzer Space Telescope and our methodology for deriving total magnitudes, stellar masses, and effective radii for 27 SLUGGS early-type galaxies. These new measurements are compared with literature values. In an Appendix we list the measurements for six additional nearby early-type galaxies, which we include for the interested reader.

2 SPITZER DATA

Here we use images from the IRAC instrument of the Spitzer Space Telescope, which has a pixel scale of 1.22 arcsec over a 5.2×5.2 arcmin⁻² field-of-view. We have downloaded the latest (July 2016) available $3.6\mu\text{m}$ basic calibrated data frames from the Spitzer Heritage Archive. These Astronomical Observation Requests (AORs) are detailed in Appendix A (for SLUGGS galaxies) and C (for non-SLUGGS galaxies). These data have been corrected for scattered light, dark current, flat-fielded and flux calibrated. The MOPEX package is used to assemble the long-exposure (>1 s) frames into an image mosaic showing the field of view around each target galaxy. An example of the final mosaic for NGC 1407 is shown in Fig. 1.

We follow a similar reduction procedure to that of Savorgnan & Graham (2016, SG16). Thus when multiple pointings are available, an overlap correction is applied to create a uniform background level. Using IRAF we determine the sky background level and rms at multiple points on the outskirts of each mosaiced image. The sky values are averaged to give a final value for the sky background of each image, which is subtracted from the image. Finally, bright stars and other unwanted objects are masked out of the mosaic. For further details see SG16.

Unfortunately, the $3.6\mu\text{m}$ data for the low-mass SLUGGS galaxy NGC 4474 are not useful for measuring the total light (and hence mass) or galaxy size. In this case, the galaxy is only partially visible as it is near the edge of the available Spitzer pointing. We therefore adopt its stellar mass ($\log M_* = 10.23$) from its 2MASS K-band magnitude and its effective radius ($R_e = 1.5$ kpc) from Brodie et al. (2014).

3 MEASURING TOTAL MAGNITUDES

To measure the total light from each galaxy we model the galaxy in 2D using the IRAF task *ellipse* and obtain the total magnitude of the galaxy model. The galaxy centre was initially allowed to vary, but if it varied by more than 1 pixel, we fixed it to the average central value. For a few galaxies (i.e. NGC 4486, 4594, 5866 and 7457) we could not obtain a good galaxy model with a radially varying position angle (PA) and so in these cases we fixed the PA to a representative value based on the radial trend. The model extends in galactocentric radius until the integrated magnitude at that radius

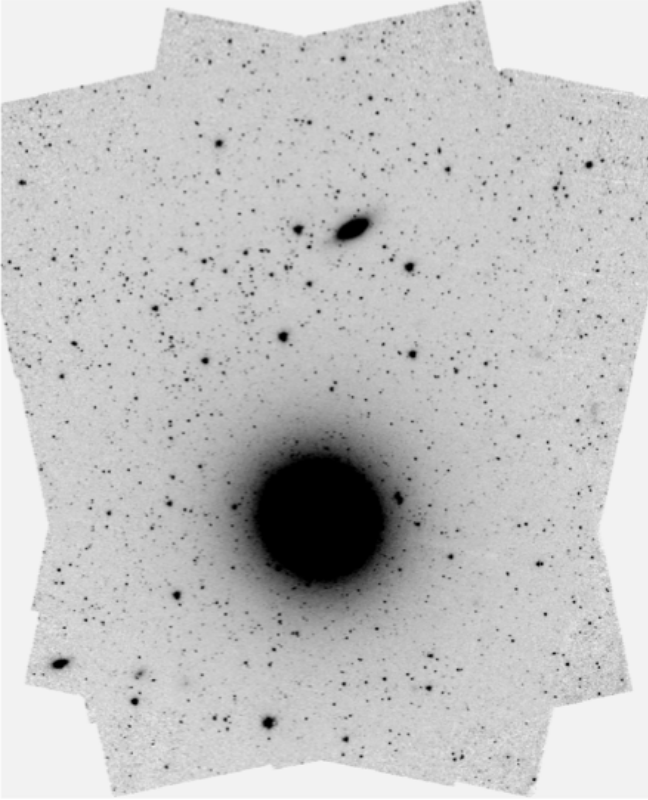


Figure 1. Spitzer Space Telescope $3.6\mu\text{m}$ image of NGC 1407. North is up and East is left. The galaxy to the North has a projected separation of 8.5 arcmins from NGC 1407.

is less than 0.02 mag different from the previous (penultimate) radius. Thus we effectively adopt the asymptotic total magnitude of the model galaxy. We estimate our combined photometric and systematic uncertainty to be ± 0.05 mag. We do not correct our $3.6\mu\text{m}$ magnitudes for Galactic extinction (which are less than 0.01 mag.). The total $3.6\mu\text{m}$ magnitudes that we measure in the Vega system, and other basic properties of the SLUGGS galaxies, are given in Table 1.

Total $3.6\mu\text{m}$ magnitudes for several SLUGGS galaxies from Spitzer data are available in the S4G study of Munoz-Mateos et al. (2015, S4G) and Savorgnan & Graham (2016, SG16). The former study measured total magnitudes using a curve-of-growth method and adopted the asymptotic magnitude. The uncertainty on the S4G total magnitudes for the SLUGGS galaxies is given as ± 0.001 – 0.002 mag. in the S4G online database. This is likely to be the formal uncertainty on fitting their asymptotic magnitude and does not include other sources of uncertainty. The latter study fit multiple components to the 1D surface brightness profile of each galaxy after 2D modelling. The combination of the different components was used to calculate the total magnitude, with an estimated uncertainty of ± 0.25 mag.

Fig. 2 shows a comparison, for the SLUGGS galaxies, of our measured magnitude against $3.6\mu\text{m}$ total magnitudes from S4G (converted to the Vega system) and SG16. Our magnitudes generally lie in between these two studies. We are systematically brighter than S4G by ~ 0.18 mag. on average. Our measurements agree fairly well with SG16 with the exception of four galaxies that are more than 0.3 mag brighter than us (and have even larger discrepan-

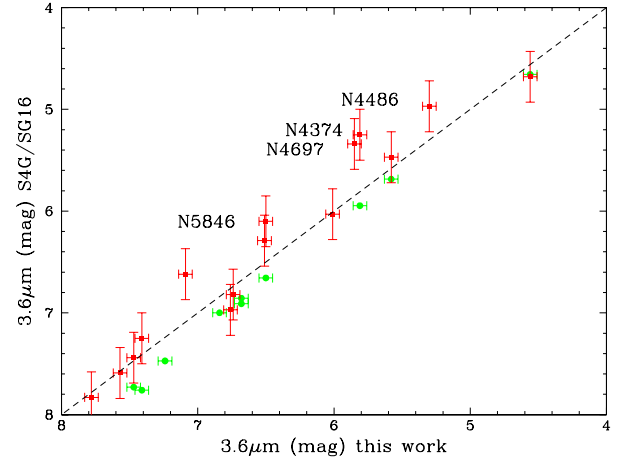


Figure 2. Comparison of $3.6\mu\text{m}$ magnitude measured in this work with the literature. Data from S4G are shown by filled green circles and SG16 by filled red squares. The dashed line shows the 1:1 line. Our $3.6\mu\text{m}$ magnitudes lie between those of S4G and SG16. Four SG16 galaxies are highlighted (see text).

cies with S4G magnitudes when in common). Three of the galaxies, NGC 5846, NGC 4374, and NGC 4486, feature a partially depleted core at their centre (Lauer et al. 2007; Krajnovic et al. 2013). The total magnitudes of SG16 do not take this into account, i.e. they masked out the core and fit a Sersic profile (rather than a core-Sersic profile) to the galaxy light. This effectively overestimates the total magnitude of each galaxy by the amount of light ‘missing’ due to the depleted core, i.e. ~ 0.2 – 0.3 mag. For NGC 4697 we suspect that the best-fit profiles of SG16 overestimated the spheroid effective radius and consequently its luminosity. Their 1D surface brightness profile for this galaxy is less extended than the best-fit effective radius itself.

4 CALCULATING TOTAL STELLAR MASSES

To calculate the total $3.6\mu\text{m}$ luminosity in solar units in the Vega system for each galaxy we convert the $3.6\mu\text{m}$ apparent magnitude into a total luminosity assuming that the absolute magnitude of the Sun to be $M_{3.6} = 3.24$ (Oh et al. 2008), and taking its distance from Table 1. We note that the distances, usually based on surface brightness fluctuations, contribute an uncertainty of ~ 0.1 dex to the luminosity.

We multiply the luminosity by the $3.6\mu\text{m}$ mass-to-light ratio from the single stellar population models of Röck et al. (2015). In particular, we use $M/L_{3.6}$ appropriate for each galaxy’s mean mass-weighted stellar age within $1 R_e$ taken from McDermid et al. (2015), supplemented by values from Rembold et al. (2005) for NGC 720, Norris et al. (2006) for NGC 3115, Spolaor et al. (2008) for NGC 1400 and 1407, and Sanchez-Blazquez et al. (2006) for NGC 4594. These ages are given in Table 1. The $3.6\mu\text{m}$ mass-to-light ratio that we apply varies from ~ 0.60 to 1.0. We use the Padova isochrones for solar metallicity (which is a reasonable value for our early-type galaxies within $1 R_e$; McDermid et al. 2015). We note that the equivalent BaSTI isochrones differ by only 0.01 for our typical age. We estimate that the uncertainty in $M/L_{3.6}$ due to differences in isochrone tracks (± 0.03), mean age uncer-

Table 1. SLUGGS galaxy sample and properties

Galaxy [NGC]	Type	Core	Dist. [Mpc]	Age [Gyr]	$m_{3.6}$ [mag]	$\log M_*$ [M_\odot]	R_e [arcsec]	μ_e [mag/arcsec ²]	n
(1)	(2)	(3)	(4)	(5)	(6)	(7)	(8)	(9)	(10)
720	E5	1	26.9	7.8	6.92	11.27	29.1	17.54	3.8
821	E6	3	23.4	12.9	7.57	11.00	43.2	19.03	6.0
1023	S0	3	11.1	13.5	6.01	10.99	48.0	17.61	4.2
1400	E1/S0	1	26.8	13.8	7.44	11.08	25.6	17.87	5.0
1407	E0	1	26.8	12.0	6.16	11.60	93.4	19.19	4.9
2768	E6/S0	2	21.8	13.3	6.68	11.21	60.3	18.70	3.8
2974	E4/S0	3	20.9	11.8	7.47	10.93	30.2	17.99	4.3
3115	S0	3	9.4	9.0	5.58	10.93	36.5	16.75	4.7
3377	E5-6	3	10.9	11.3	7.09	10.50	45.4	18.81	5.9
3607 [†]	S0	1	22.2	13.5	6.51	11.39	48.2	18.33	5.3
3608	E1-2	1	22.3	13.0	7.41	11.03	42.9	19.00	5.3
4111	S0	–	14.6	6.0	7.24	10.52	10.1	15.71	3.0
4278	E1-2	1	15.6	13.7	6.84	10.95	28.3	17.51	6.2
4365	E3	1	23.1	13.4	6.31	11.51	77.8	18.96	4.9
4374	E1	1	18.5	13.7	5.81	11.51	139.0	19.71	8.0
4459	S0	3	16.0	11.9	6.76	10.98	48.3	18.52	5.4
4473	E5	1	15.2	13.0	6.74	10.96	30.2	17.67	5.0
4474	S0	3	15.5	11.1	–	10.23	17.0	–	–
4486	E0/cD	1	16.7	12.7	5.30	11.62	86.6	18.24	5.1
4494	E1-2	3	16.6	11.0	6.68	11.02	52.5	18.53	4.5
4526	S0	–	16.4	13.6	6.17	11.26	32.4	17.05	3.6
4564	E6	3	15.9	13.3	7.78	10.58	14.8	16.93	3.2
4594 [†]	Sa	1	9.5	12.5	4.56	11.41	72.0	17.06	3.2
4649	E2/S0	1	16.5	13.2	5.33	11.60	79.2	18.06	4.6
4697	E6	3	12.5	13.4	5.85	11.15	95.8	19.08	5.3
5846	E0-1/S0	1	24.2	12.7	6.50	11.46	89.8	19.38	5.2
5866 [†]	S0	–	14.9	5.9	6.50	10.83	23.4	16.59	2.8
7457	S0	3	12.9	6.1	7.94	10.13	34.1	18.67	2.6

Notes: columns are (1) galaxy name, [†] = bonus galaxy, (2) Hubble type, (3) 1 = core, 2 = intermediate, 3 = cusp central light profile, (4) distance from B14 (typical uncertainty is ± 0.05 dex), (5) mean stellar age from McDermid et al. (2015), see text for exceptions, (6) 3.6 micron apparent magnitude in the Vega system (typical uncertainty is ± 0.05), (7) stellar mass (typical uncertainty is ± 0.1 dex), (8) effective radius (typical uncertainty is $+0.18$ and -0.13 dex), (9) μ_e (typical uncertainty is $+0.52$ and -1.11 mag.), (10) Sersic n (typical uncertainty is $+0.13$ and -0.11 dex). Spitzer $3.6\mu\text{m}$ imaging is not available for NGC 4474: M_* and R_e are from 2MASS $2.2\mu\text{m}$ imaging.

tainty (± 0.05) and metallicity variations (± 0.02), combined with our measurement and distance uncertainties, give a final uncertainty of about 0.1 dex in log stellar mass. We also assume a Kroupa IMF. As noted in the Introduction, although there is evidence for an IMF skewed to low mass stars, the effect seems largely limited to the central regions of the most massive galaxies. Nevertheless this gives rise to a systematic underestimate of the stellar masses of the most massive galaxies.

Each galaxy in this study has a total stellar mass determined from the total K-band ($2.2\mu\text{m}$) magnitude from the 2MASS survey. The 2MASS $2.2\mu\text{m}$ magnitude is corrected for missing flux according to Scott et al. (2013) and we take the absolute magnitude of the Sun to be $M_{2.2} = 3.28$ (table 2.1 from Binney & Merrifield 1998). The stellar mass has been calculated in previous SLUGGS papers assuming a fixed $M/L_{2.2} = 1.0$ irrespective of stellar age (e.g. Alabi et al. 2016). A value of unity is reasonably representative of an old, metal-rich stellar population with a Kroupa-like IMF.

In Fig. 3 we show a comparison of our new $3.6\mu\text{m}$ -based stellar masses versus the stellar mass obtained from the K-band. We find an excellent overall correspondence with the stellar masses derived using the K-band. Galaxies with lower $3.6\mu\text{m}$ masses relative to the previous $2.2\mu\text{m}$ masses (i.e. that lie above the unity line) tend to be those with young (~ 6 Gyr) mean stellar ages. The overall ex-

cellent agreement indicates that both $3.6\mu\text{m}$ and $2.2\mu\text{m}$ total magnitudes give reliable stellar masses (under the same assumption of a Kroupa IMF). Given the small difference in 2.2 vs $3.6\mu\text{m}$ stellar masses, we will continue to adopt the K-band stellar mass of $\log M_* = 10.23$ for NGC 4474 for which we are unable to measure a $3.6\mu\text{m}$ magnitude.

5 MEASURING GALAXY SIZES

Each galaxy surface brightness profile is fit with a single Sersic law (Graham & Driver 2005). We exclude the inner 2 pixels (2.44 arcsec), i.e. we only fit radii that are larger than the effective FWHM resolution of the Spitzer Space Telescope. This also means that the presence of any nuclear star cluster or AGN does not affect the fits. Most of our galaxies reveal central surface brightness profiles that can be well described as either a core or a cusp (Lauer et al. 2007; Krajnovic et al. 2013; Dullo & Graham 2013), as listed in Table 1. In the case of cusps, they are generally well fit by a single Sersic profile. On the other hand for core profiles we exclude the so-called depleted core region from the fits. Thus the fitting range for each galaxy is either >2 pixels for the cusp, intermediate and

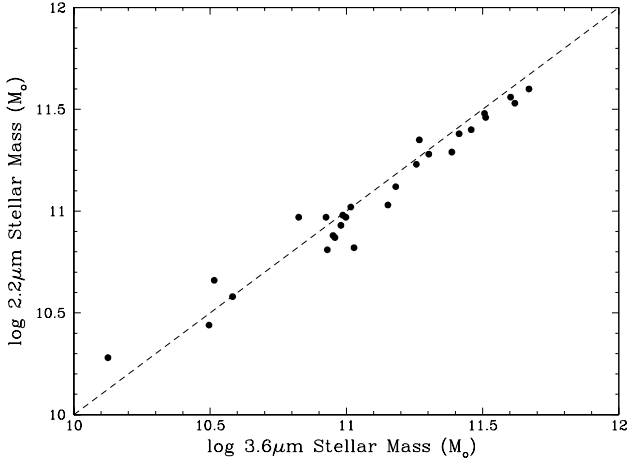


Figure 3. Comparison of $3.6\mu\text{m}$ stellar mass measured in this work with the K-band ($2.2\mu\text{m}$) stellar mass. The dashed line shows the 1:1 line.

unknown galaxies and greater than the depleted core region for the core galaxies.

The fits to the $3.6\mu\text{m}$ surface brightness profile for each SLUGGS galaxy are shown in Appendix B. The central region excluded from each fit is indicated by open circles, and can be most clearly seen in the Sersic profile minus data residual profiles. The code used for the fitting process is the same as SG16. For most galaxies SG16 fit multiple components to each galaxy. However, they did fit a single Sersic profile to three large SLUGGS galaxies. In these cases our effective radii agree very well with their value, i.e. NGC 4374: 139.0 vs 129.8 arcsec, NGC 4486: 86.6 vs 87.1 arcsec and NGC 5846: 89.8 vs 83.4 arcsec.

We list the (equivalent circular) effective radii from the single Sersic fits to our $3.6\mu\text{m}$ surface brightness profiles in Table 1. A typical uncertainty associated with the effective radius of the SLUGGS galaxies is calculated based on the average of the uncertainties of the 14 early-type galaxies effective radii in the sample of SG16 with single Sersic fits compared to those from other studies (see SG16 for details). The 1σ uncertainty of +0.18 dex and -0.13 dex thus takes into account both random and systematic errors. If we only considered random measurement errors a smaller uncertainty would result. Table 1 also lists the other fitting parameters, i.e. the Sersic n value and the surface brightness at the effective radius μ_e . Again, we adopt the typical uncertainties found for the 14 early-type galaxies, i.e. +0.13 and -0.11 dex on n , and +0.52 and -1.11 mag on μ_e . We note that Sersic parameters are strongly correlated with each other.

In Fig. 4 we compare our new effective radii from the Spitzer images with those listed by Brodie et al. (2014), i.e. from Cappellari et al. (2011), based on optical data. We find good correspondence for small-sized galaxies and generally we measure greater effective radii for the large-sized galaxies. This implies that the sizes of the most massive galaxies are underestimated, as was suggested by Cappellari et al. (2011). Given the reasonable agreement in sizes for the smaller galaxies, the uncertainties from the work of SG16 may be an overestimate.

Fig. 4 also shows the effective radii from the 2MASS Large Galaxy Atlas (Jarrett et al. 2003). In particular, we take the K-band effective radius along the semi-major axis ($k_{r,eff}$) and multiply it by an ellipticity correction ($\sqrt{k_{ba}}$) to obtain an equivalent cir-

Table 2. Massive Galaxy Sizes

Galaxy	$3.6\mu\text{m}$	B14	Kor09	Chen10	Vika13	Other
[NGC]	[arcsec]	[arcsec]	[arcsec]	[arcsec]	[arcsec]	
(1)	(2)	(3)	(4)	(5)	(6)	(7)
1407	93	63	–	–	–	100 (P15)
4365	78	53	~ 154	97	78	126 (B12)
4374	139	53	~ 135	131	96	–
4486	87	81	~ 630	105	82	–
4649	79	66	~ 118	105	68	–
5846	90	59	–	–	–	81 (N14)

Notes: columns are (1) galaxy name, effective radii in arcsec from (2) $3.6\mu\text{m}$ imaging (this work), (3) Brodie et al. (2014), (4) Kormendy et al. (2009), (5) Chen et al. (2010), (6) Vika et al. (2013), and (7) other published SLUGGS works (i.e. Pota et al. 2015; Blom et al. 2012 and Napolitano et al. 2014).

cular R_e value. Cappellari et al. (2011) found that the 2MASS effective radii were on average $1.7\times$ smaller than the optical radii from the RC3. The dotted line in this plot indicates sizes reduced by this factor and indeed the 2MASS R_e values scatter about this line. The smaller sizes may be due to an over-subtraction of the sky background which truncates the 2MASS K-band surface brightness profile (Schombert & Smith 2012).

We find that both the 2MASS and B14 effective radii underestimate the true size of the most massive, largest galaxies. In Table 2 we list R_e values in arcsec from single Sersic fits to the surface brightness profiles of the six most massive SLUGGS galaxies from the literature, along with the B14 values and those measured in this work. We include the single Sersic fits to SDSS imaging from Chen et al. (2010) and Vika et al. (2013). In the case of Vika et al. we quote the z band R_e value. The final column in Table 2 gives R_e values derived by previous SLUGGS studies of Blom et al. (2012) and Pota et al. (2015) from deep optical imaging, and that adopted by Napolitano et al. (2014).

We also include effective radii from Kormendy et al. (2009) who presented very deep optical imaging from multiple sources of Virgo cluster galaxies, and fit single Sersic profiles excluding the central core region (as we have done). We have converted their semi-major axis effective radii to equivalent circular ones using each galaxy’s average ellipticity. We also have four low mass Virgo galaxies in common with Kormendy et al. and we find good agreement for three (NGC 4473, 4564 and 4551), For NGC 4459 we find a somewhat larger size than Kormendy et al. (2009) but this galaxy is difficult to model correctly given the bright nearby foreground star (despite our efforts to mask it from the 2D modelling process).

For the massive Virgo galaxies, we have excellent agreement for NGC 4374 (M84) with Kormendy et al. and Chen et al. For NGC 4365, 4486 and 4649 (M60), we have good agreement with Vika et al., but we find systematically smaller sizes than Chen et al., and significantly smaller sizes than Kormendy et al. (and Blom et al. 2012 for NGC 4365). We suspect that this is because these galaxies have elongated isophotes in their outer regions, i.e light that goes beyond the Spitzer mosaic (whereas NGC 4374 has very circular outer isophotes and is well contained within our mosaic). For NGC 4486 (M87) Kormendy et al. derive a size that is $6\text{--}8\times$ that of other studies (corresponding to ~ 50 kpc). Their single Sersic fit includes the extended light of the cD envelope. Our measured $3.6\mu\text{m}$ effective radii for NGC 1407 and NGC 5846 are similar to

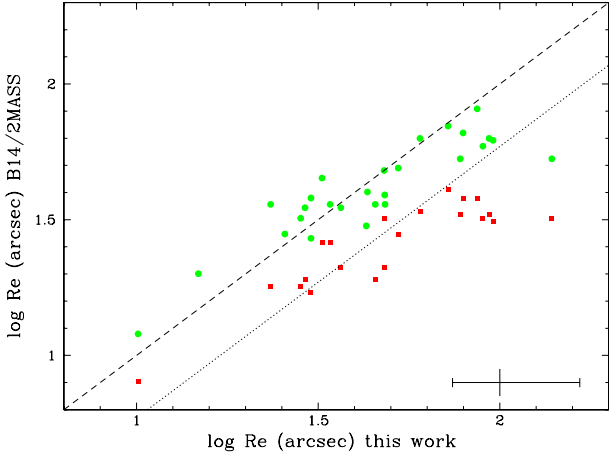


Figure 4. Comparison of the $3.6\mu\text{m}$ effective radius measured in this work with other works. The optical-based sizes used by Brodie et al. (2014, B14) are shown by filled green circles, and sizes from the near-IR 2MASS LGA are shown by filled red squares. The dashed line shows the 1:1 line, whereas the dotted line shows a reduction by a factor of $1.7\times$ from the unity relation. A typical error bar for our effective radii measurements is shown at lower right. The optical and 2MASS near-IR sizes of the large galaxies appear to be underestimated.

those used by Pota et al. (2015) and Napolitano et al. (2014) but significantly larger than B14.

We compare our $3.6\mu\text{m}$ sizes and stellar masses with the Virgo cluster galaxies of Chen et al. (2010) in Fig. 5. Chen et al. fit single Sersic profiles to multi-filter SDSS imaging of ~ 100 Virgo cluster early-type galaxies. We convert their measurements into physical properties assuming a Virgo distance of 16.5 Mpc, and $\log M/L_g = 0.7$ from Bell et al. (2003) for red galaxies. Fig. 5 shows that the distribution of sizes and stellar masses from our $3.6\mu\text{m}$ measurements for the SLUGGS galaxies are consistent with that of the Virgo early-type galaxies from Chen et al. (2010). Thus we expect our new stellar masses and effective radii for the SLUGGS galaxies to be representative of nearby early-type galaxies in general.

It is clear from Table 2 that a wide variety of galaxy effective radii can be found in the literature for massive galaxies (even when restricted to a single Sersic fit). We recognise that our effective radii derived from Spitzer $3.6\mu\text{m}$ imaging may be updated by deeper imaging studies (perhaps leading to even larger R_e values if a single Sersic continues to be adopted), however our Spitzer imaging provides a homogenous set of improved effective radii for the SLUGGS survey which we now adopt.

6 CONCLUSIONS

Using archival Spitzer Space Telescope imaging of the nearby early-type galaxies from the SLUGGS survey, we have created $3.6\mu\text{m}$ mosaic images of each galaxy (excluding NGC 4474 for which Spitzer imaging was not available). After masking out foreground stars and other unwanted features, we modelled each galaxy and derived total asymptotic magnitudes. Our total magnitudes generally lie in between those of $3.6\mu\text{m}$ literature studies for the galaxies in common. These total magnitudes are converted into stellar masses using the single stellar population models of Röck et al. (2015). The $3.6\mu\text{m}$ flux from early-type galaxies is an ideal

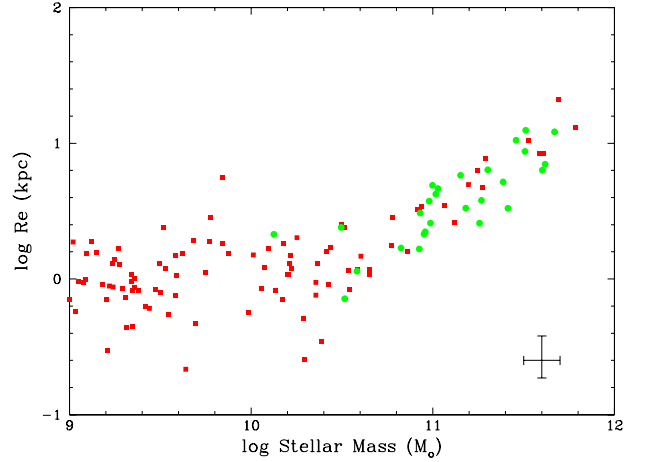


Figure 5. Size-mass distribution. We show data from Chen et al. (2010) as filled red squares and measurements from this work using the Spitzer Space Telescope imaging as filled green circles. A typical errorbar is shown lower right. Overall the two distributions are very similar.

tracer of stellar mass as the mass-to-light ratio at this wavelength is very insensitive to metallicity and only mildly sensitive to age for old stellar populations. Here we use $M/L_{3.6}$ from Padova isochrones that is adjusted for each galaxy’s mean stellar age while assuming a Kroupa IMF. We estimate the final uncertainty in log stellar mass to be ± 0.1 dex. We find that our $3.6\mu\text{m}$ stellar masses have a strong linear correlation with stellar masses derived at $2.2\mu\text{m}$, after correcting the 2MASS K-band fluxes for missing light.

From our 2D galaxy modelling, we fit a single Sersic law to the $3.6\mu\text{m}$ surface brightness profile in 1D. We exclude the central 2 pixels in all galaxies (corresponding to the FWHM of the Spitzer Space Telescope) and in addition exclude the central core of the massive galaxies that contain so-called depleted cores. As well as new effective radii (R_e), we derive the surface brightness at $1 R_e$ and the Sersic n parameter. Our $3.6\mu\text{m}$ sizes show good agreement with literature values from optical imaging as used by Brodie et al. (2014), and show that sizes from the 2MASS (K-band) survey systematically underestimate the true size (as found previously by Cappellari et al. 2011). For the larger, more massive galaxies we find that the optical sizes used by Brodie et al. (2014) are also systematically underestimated relative to the sizes from our $3.6\mu\text{m}$ imaging and deep optical imaging in the literature. Our new sizes and stellar masses show good agreement with those of Virgo cluster early-type galaxies measured from SDSS imaging. We now adopt the sizes and stellar masses, measured in a homogeneous way from our $3.6\mu\text{m}$ imaging, for galaxies in the SLUGGS survey. Our methodology can be adopted by other studies requiring more accurate effective radii and stellar masses for nearby early-type galaxies.

7 ACKNOWLEDGEMENTS

We thank A. Ferre-Mateu and A. Alabi for useful comments. We thank the referee for several suggestions that have improved the paper. DAF thanks the ARC for financial support via DP130100388. JB and AR acknowledge NSF grants AST-1211995, AST-1616598 and AST-1616710. This work is based on observations made with the Spitzer Space Telescope, which is operated by the Jet Propul-

sion Laboratory, California Institute of Technology under a contract with NASA.

8 REFERENCES

- Alabi A. B., et al., 2015, MNRAS, 452, 2208
 Arnold J. A., et al., 2014, ApJ, 791, 80
 Binney J., Merrifield M., 1998, Galactic Astronomy, Princeton University Press
 Blom C., Spitler L. R., Forbes D. A., 2012, MNRAS, 420, 37
 Brodie J. P., et al., 2014, ApJ, 796, 52 (B14)
 Bruzual G., Charlot S., 2003, MNRAS, 344, 1000
 Cappellari M., et al., 2011, MNRAS, 413, 813
 Chen C.-W., Côté P., West A. A., Peng E. W., Ferrarese L., 2010, ApJS, 191, 1
 Conroy C., Gunn J. E., 2010, ApJ, 712, 833
 Cushing M. C., Rayner J. T., Vacca W. D., 2005, ApJ, 623, 1115
 Dullo B. T., Graham A. W., 2013, ApJ, 768, 36
 Ferré-Mateu A., Vazdekis A., de la Rosa I. G., 2013, MNRAS, 431, 440
 Foster C., et al., 2016, MNRAS, 457, 147
 Graham A. W., Driver S. P., 2005, PASA, 22, 118
 Jarrett T. H., Chester T., Cutri R., Schneider S. E., Huchra J. P., 2003, AJ, 125, 525
 Kormendy J., Fisher D. B., Cornell M. E., Bender R., 2009, ApJS, 182, 216
 Krajnović D., et al., 2013, MNRAS, 433, 2812
 Lauer T. R., et al., 2007, ApJ, 664, 226
 Martín-Navarro I., Barbera F. L., Vazdekis A., Falcón-Barroso J., Ferreras I., 2015, MNRAS, 447, 1033
 Meidt S. E., et al., 2012, ApJ, 744, 17
 Meidt S. E., et al., 2014, ApJ, 788, 144
 McConnell N. J., Lu J. R., Mann A. W., 2016, ApJ, 821, 39
 McDermid R. M., et al., 2015, MNRAS, 448, 3484
 Milone A. D. C., Rickes M. G., Pastoriza M. G., 2007, A&A, 469, 89
 Muñoz-Mateos J. C., et al., 2015, ApJS, 219, 3 (S4G)
 Napolitano N. R., Pota V., Romanowsky A. J., Forbes D. A., Brodie J. P., Foster C., 2014, MNRAS, 439, 659
 Norris M. A., Sharples R. M., Kuntschner H., 2006, MNRAS, 367, 815
 Norris M. A., Meidt S., Van de Ven G., Schinnerer E., Groves B., Querejeta M., 2014, ApJ, 797, 55
 Oh S.-H., de Blok W. J. G., Walter F., Brinks E., Kennicutt R. C., Jr., 2008, AJ, 136, 2761
 Pota V., et al., 2015, MNRAS, 450, 3345
 Querejeta M., et al., 2015, ApJS, 219, 5
 Rayner J. T., Cushing M. C., Vacca W. D., 2009, ApJS, 185, 289
 Rembold S. B., Pastoriza M. G., Bruzual G., 2005, A&A, 436, 57
 Röck B., Vazdekis A., Peletier R. F., Knapen J. H., Falcón-Barroso J., 2015, MNRAS, 449, 2853
 Sanchez-Blazquez P., Gorgas J., Cardiel N., Gonzalez J. J., 2006, A&A, 457, 809
 Savorgnan G. A. D., Graham A. W., 2016, ApJS, 222, 10 (SG16)
 Schombert J., Smith A. K., 2012, PASA, 29, 174
 Scott N., Graham A. W., Schombert J., 2013, ApJ, 768, 76
 Spolaor M., Forbes D. A., Proctor R. N., Hau G. K. T., Brough S., 2008, MNRAS, 385, 675
 Vika M., Bamford S. P., Häußler B., Rojas A. L., Borch A., Nichol R. C., 2013, MNRAS, 435, 623
 Villaume A., Conroy C., Johnson B. D., 2015, ApJ, 806, 82

- Werner M. W., et al., 2004, ApJS, 154, 1
 Wright E. L., et al., 2010, AJ, 140, 1868
 van den Bosch R., 2016, arXiv:1606.01246

9 APPENDIX A

Summary of Astronomical Observation Requests (AORs) of SLUGGS galaxies downloaded in July 2016 from the Spitzer Heritage Archive (<http://sha.ipac.caltech.edu>) are given in Table 3.

10 APPENDIX B

Sersic fits to $3.6\mu\text{m}$ surface brightness profiles of SLUGGS galaxies are shown in Figures 6 to 14.

11 APPENDIX C

Six additional (non-SLUGGS) galaxies have been measured in this study using the procedure described above. In Table 4 we list the Astronomical Observation Requests and in Table 5 the measured $3.6\mu\text{m}$ properties for these additional galaxies. Figures 15 and 16 show Sersic fits to their $3.6\mu\text{m}$ surface brightness profiles.

Table 3. Spitzer Space Telescope Astronomical Observation Requests for SLUGGS Galaxies

Galaxy [NGC]	Astronomical Observation Requests
720	r49345024, r49345280
821	r14569216, r49418752, r49419008
1023	r4432640, r50631168, r50631680, r50631936, r52778496, r52778752, r52779008, r52779264, r52779520, r52779776, r52780032
1400	r49436416
1407	r49348096, r49348352
2768	r18031872
2974	r18032384, r49613056
3115	r4441088
3377	r4444928, r49411328, r50545664, r50545920, r50546176, r52910336, r52910592, r52910848, r52911104, r52911360, r52911616, r52911872
3607	r4449536, r49389312, r49614592, r49614848
3608	r18033408, r49460736, r49614848
4111	r30984192, r31015424, r42249216, r42249472, r50528000, r50528256, r50528512, r52912128, r52912384, r52912640, r52912896, r52913152, r52913408
4278	r4461568, r49616128
4365	r11115264, r49358336, r49358592, r50576640, r50577152, r50577664, r52976640, r52976896, r52977152, r52977408, r52977664, r52977920
4374	r4463872, r50608128, r50608640, r50609152, r52971264, r52971520, r52971776, r52972032, r52972288, r52972544
4459	r11378944, r49501696, r49501952
4473	r11377920, r49339904, r49340160, r50554368, r50554880, r50555392, r53005312, r53005568, r53005824, r53006080, r53006336, r53006592
4474	–
4486	r12673792, r49337856, r49338112, r50576384, r50576896, r50577408, r52962304, r52962560, r52962816, r52963072, r52963328, r52963584
4494	r18035200
4526	r4472064, r49341440, r49341696, r49595904, r50644736, r50644992, r50645248, r52992768, r52993024, r52993280, r52993792, r52994048
4564	r14572032, r49510912, r49511168, r50647040, r50647296, r50647552, r52942592, r52942848, r52943104, r52943360, r52943616, r52943872
4594	r5517824, r5518080, r50595328, r50595840, r50596864, r52765696, r52765952, r52766208, r52766464, r52766720, r52766976, r52767232
4649	r4476672, r49337344, r49337600, r50590208, r50590976, r50591488, r52967680, r52967936, r52968192, r52968448, r52968704, r52968960
4697	r10896896, r49359872, r49360128, r50622464, r50622720, r50622976, r52809472, r52809728, r52809984, r52810240, r52810496, r52810752, r52811008
5846	r4491264, r16310272, r49363968, r49364224
5866	r5526016, r5526272
7457	r18037504, r50547200, r50547456, r50547712, r52946176, r52946432, r52946688, r52946944, r52947200, r52947456

Table 4. Spitzer Space Telescope Astronomical Observation Requests for non-SLUGGS Galaxies

Galaxy [NGC]	Astronomical Observation Requests
1052	r11516672, r49600512, r49612288
2549	r26602240, r49447424, r49447680, r49619712
3379	r4445696, r49411584, r49411840, r50629376, r50629632, r50629888, r52832512, r52832768, r52833024, r52833280, r52833536, r52833792, r52834048
3665	r49465344, r49465600
3998	r4452608, r42242560, r42242816, r49622784, r50586368, r50586624, r50586880, r52892416, r52892672, r52892928, r52893184, r52893440, r52893696
4551	r49510400, r49510656

Table 5. Non-SLUGGS galaxy properties

Galaxy [NGC]	Type	Core	Dist. [Mpc]	Age [Gyr]	m _{3,6} [mag]	M _* [M _⊙]	R _e [arcsec]	μ _e [mag/arcsec ²]	n
(1)	(2)	(3)	(4)	(5)	(6)	(7)	(8)	(9)	(10)
1052	E3-4/S0	1	19.4	13.0	7.12	11.02	21.9	17.16	3.4
2549	S0	3	12.3	8.9	7.75	10.28	14.7	16.88	3.1
3379	E0-1	1	10.3	13.7	5.92	10.96	54.9	18.02	5.7
3665	S0	–	33.1	13.2	7.12	11.48	50.5	18.95	5.4
3998	S0	2	13.7	13.7	7.04	10.76	19.1	16.92	4.0
4551	E	3	16.1	13.2	8.67	10.24	13.8	17.45	2.1

Notes: columns are (1) galaxy name, (2) Hubble type, (3) 1= core, 2 = intermediate, 3 = cusp central light profile, (4) distance, (5) mean stellar age from McDermid et al. (2015), except for NGC 1052 from Milone et al. (2007), (6) 3.6 micron apparent mag., (7) stellar mass, (8) effective radius, (9) μ_e, (10) Sersic n.

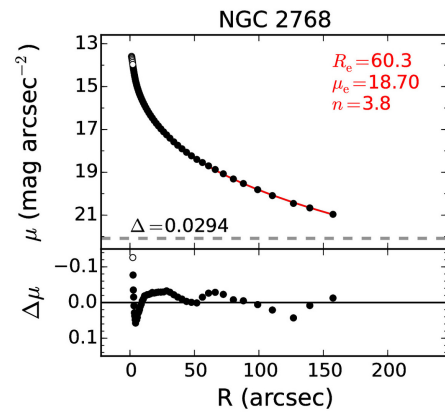
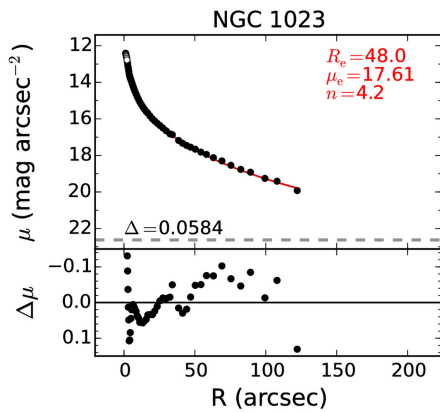
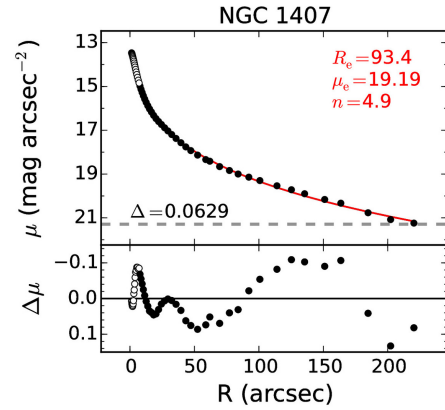
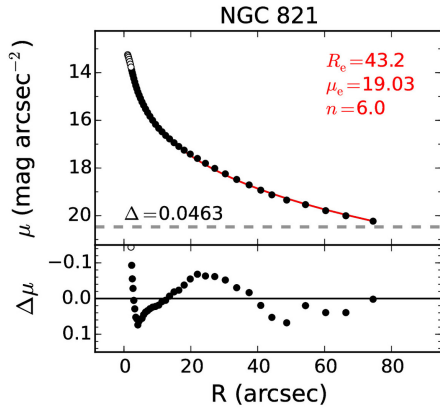
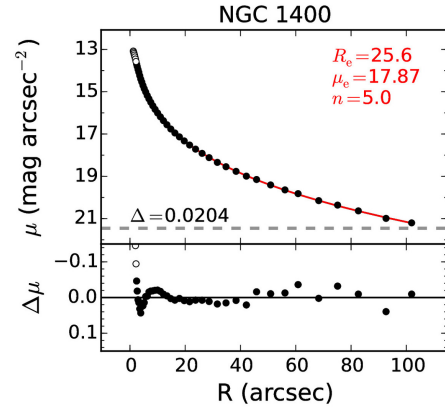
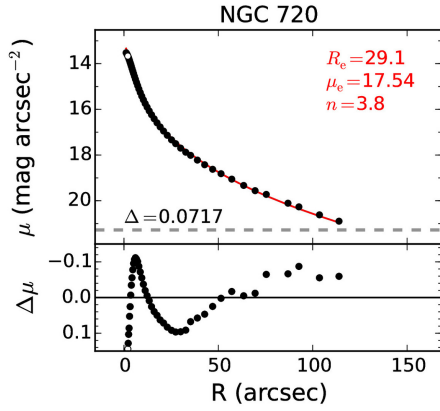


Figure 6. Sersic fit to $3.6\mu\text{m}$ surface brightness profile and residuals as a function of circular equivalent radius. The *upper* panel shows the data points (with excluded data points shown by open circles) and the best fit Sersic profile in red. Parameters for the Sersic fit are given in the top right. The dashed line shows $3\times$ the rms of the sky background level. Δ gives the rms of the residuals in mag arcsec^{-2} . The *lower* panel shows the residuals of the Sersic model fit minus the surface brightness data.

Figure 7. Sersic fit to $3.6\mu\text{m}$ surface brightness profile and residuals as a function of circular equivalent radius. The *upper* panel shows the data points (with excluded data points shown by open circles) and the best fit Sersic profile in red. Parameters for the Sersic fit are given in the top right. The dashed line shows $3\times$ the rms of the sky background level. Δ gives the rms of the residuals in mag arcsec^{-2} . The *lower* panel shows the residuals of the Sersic model fit minus the surface brightness data.

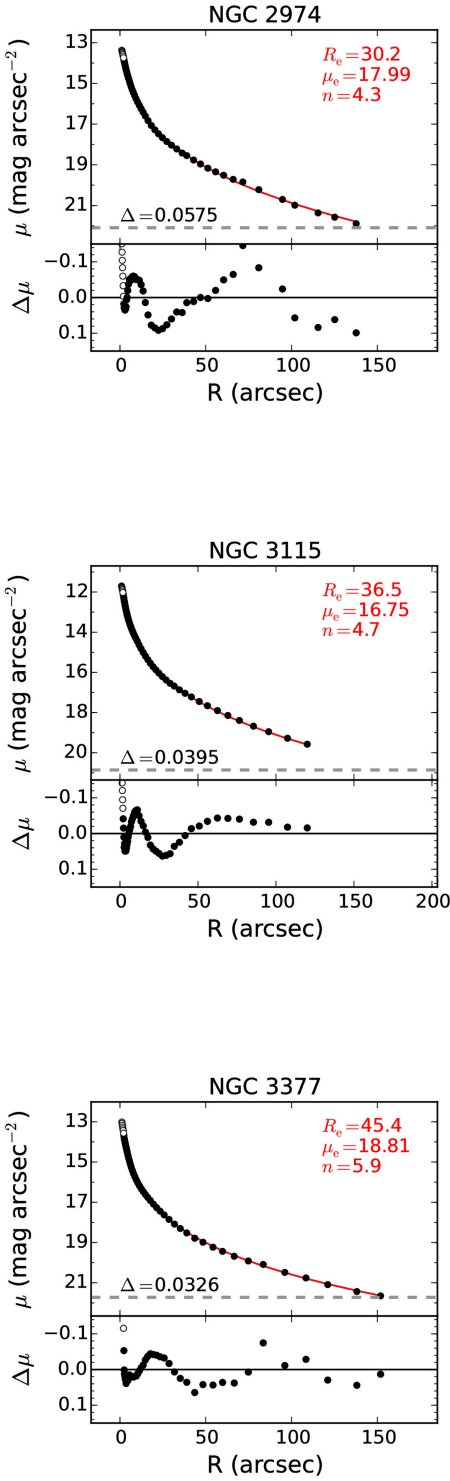


Figure 8. Sersic fit to $3.6\mu\text{m}$ surface brightness profile and residuals as a function of circular equivalent radius. The *upper* panel shows the data points (with excluded data points shown by open circles) and the best fit Sersic profile in red. Parameters for the Sersic fit are given in the top right. The dashed line shows $3 \times$ the rms of the sky background level. Δ gives the rms of the residuals in mag arcsec $^{-2}$. The *lower* panel shows the residuals of the Sersic model fit minus the surface brightness data.

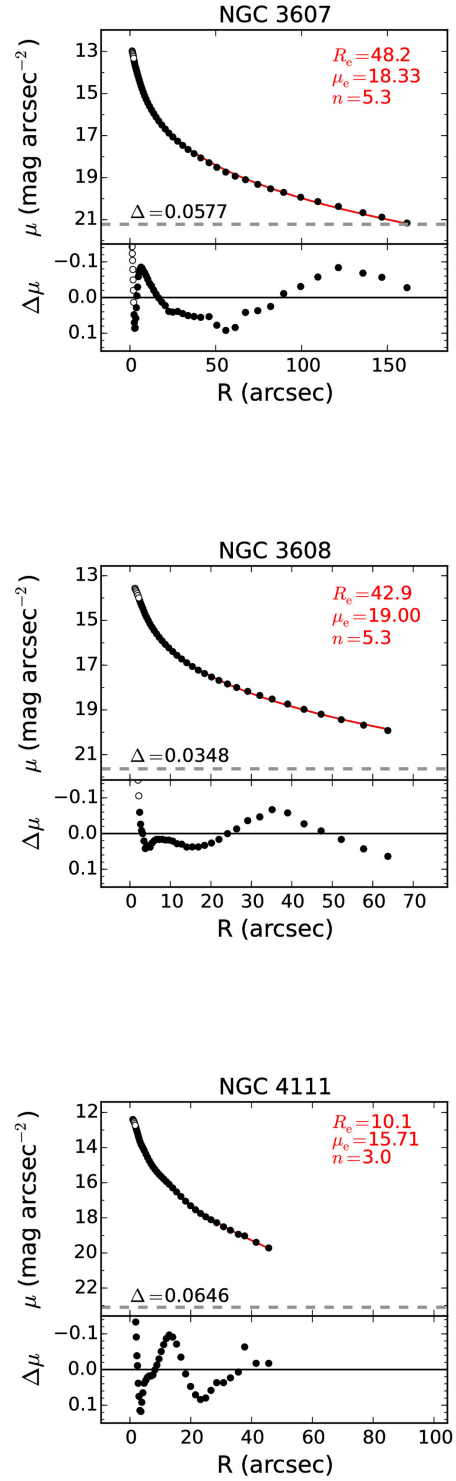


Figure 9. Sersic fit to $3.6\mu\text{m}$ surface brightness profile and residuals as a function of circular equivalent radius. The *upper* panel shows the data points (with excluded data points shown by open circles) and the best fit Sersic profile in red. Parameters for the Sersic fit are given in the top right. The dashed line shows $3 \times$ the rms of the sky background level. Δ gives the rms of the residuals in mag arcsec $^{-2}$. The *lower* panel shows the residuals of the Sersic model fit minus the surface brightness data.

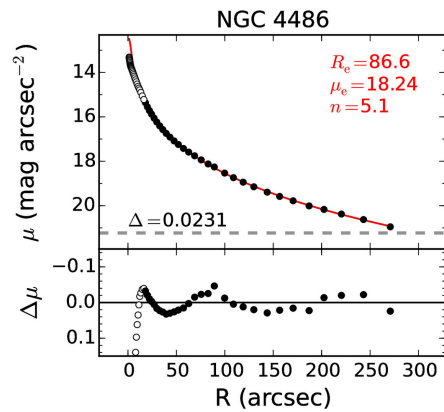
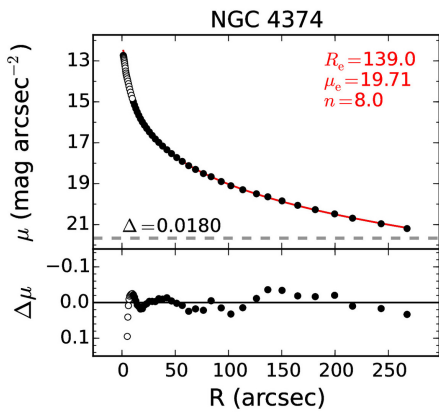
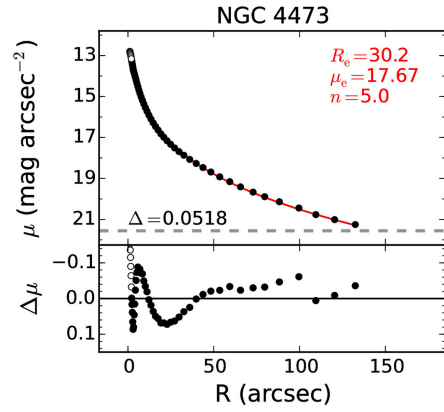
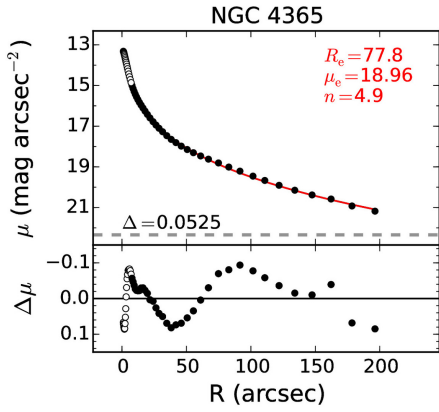
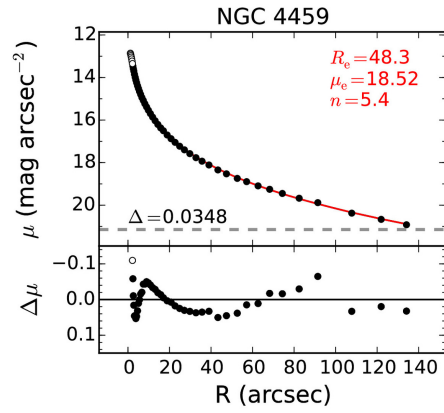
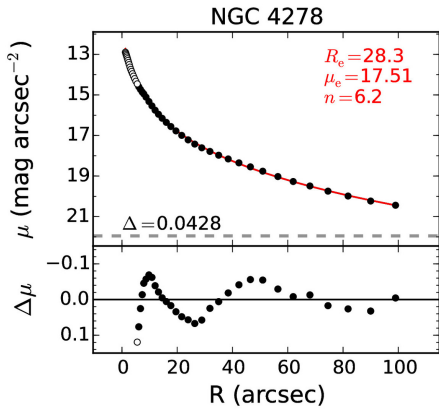


Figure 10. Sersic fit to $3.6\mu\text{m}$ surface brightness profile and residuals as a function of circular equivalent radius. The *upper* panel shows the data points (with excluded data points shown by open circles) and the best fit Sersic profile in red. Parameters for the Sersic fit are given in the top right. The dashed line shows $3\times$ the rms of the sky background level. Δ gives the rms of the residuals in mag arcsec^{-2} . The *lower* panel shows the residuals of the Sersic model fit minus the surface brightness data.

Figure 11. Sersic fit to $3.6\mu\text{m}$ surface brightness profile and residuals as a function of circular equivalent radius. The *upper* panel shows the data points (with excluded data points shown by open circles) and the best fit Sersic profile in red. Parameters for the Sersic fit are given in the top right. The dashed line shows $3\times$ the rms of the sky background level. Δ gives the rms of the residuals in mag arcsec^{-2} . The *lower* panel shows the residuals of the Sersic model fit minus the surface brightness data.

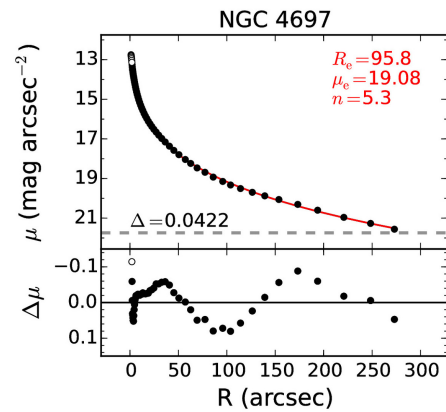
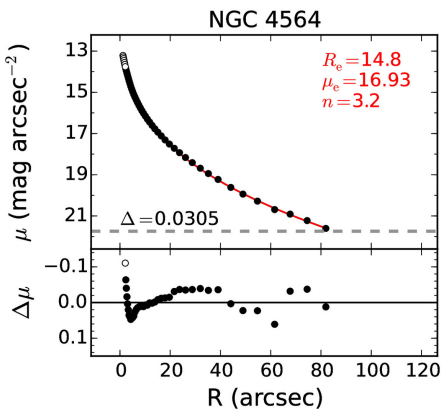
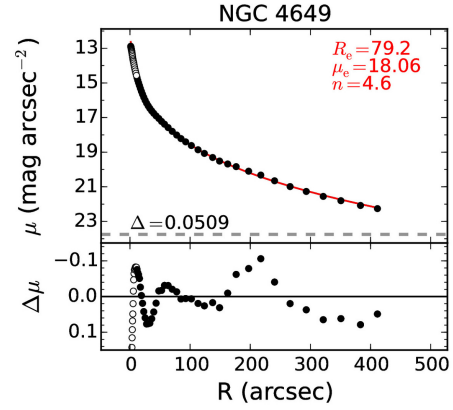
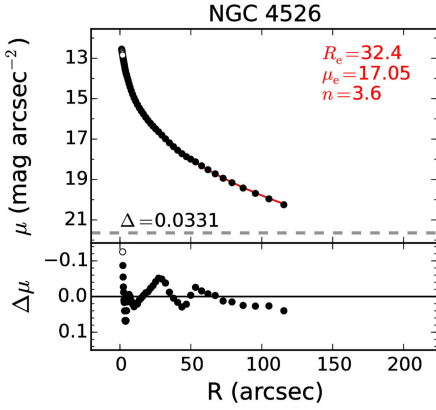
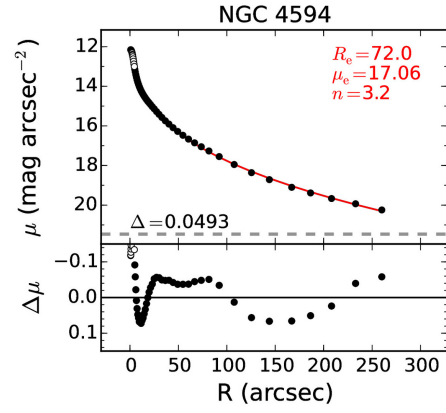
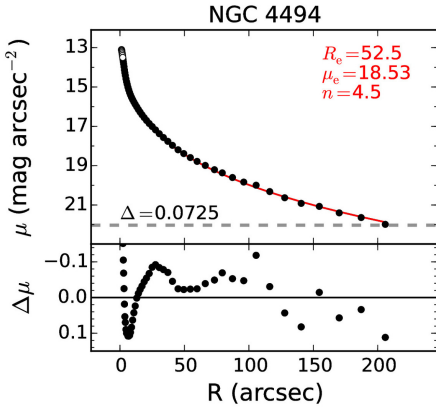


Figure 12. Sersic fit to $3.6\mu\text{m}$ surface brightness profile and residuals as a function of circular equivalent radius. The *upper* panel shows the data points (with excluded data points shown by open circles) and the best fit Sersic profile in red. Parameters for the Sersic fit are given in the top right. The dashed line shows $3\times$ the rms of the sky background level. Δ gives the rms of the residuals in mag arcsec^{-2} . The *lower* panel shows the residuals of the Sersic model fit minus the surface brightness data.

Figure 13. Sersic fit to $3.6\mu\text{m}$ surface brightness profile and residuals as a function of circular equivalent radius. The *upper* panel shows the data points (with excluded data points shown by open circles) and the best fit Sersic profile in red. Parameters for the Sersic fit are given in the top right. The dashed line shows $3\times$ the rms of the sky background level. Δ gives the rms of the residuals in mag arcsec^{-2} . The *lower* panel shows the residuals of the Sersic model fit minus the surface brightness data.

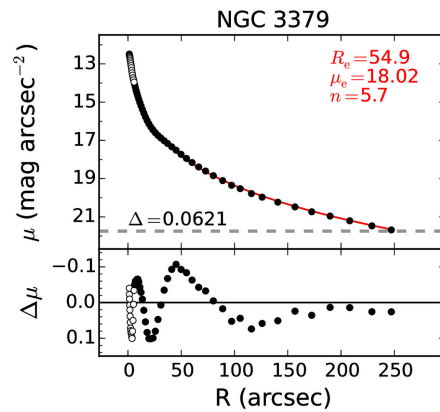
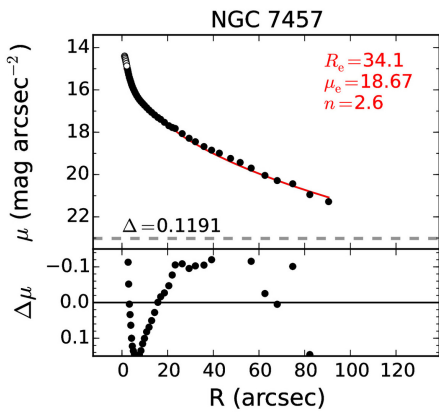
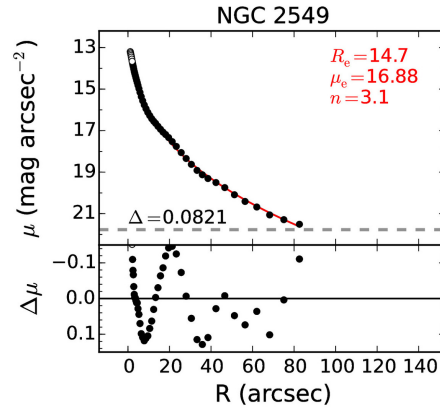
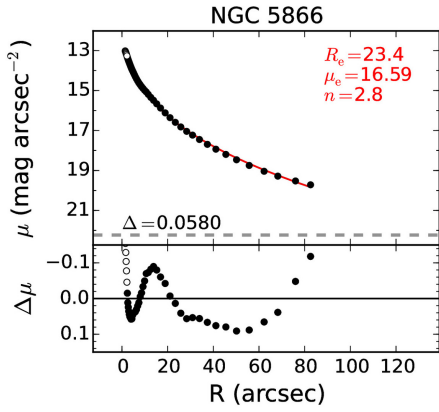
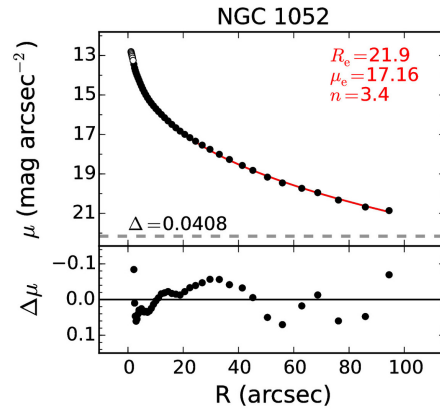
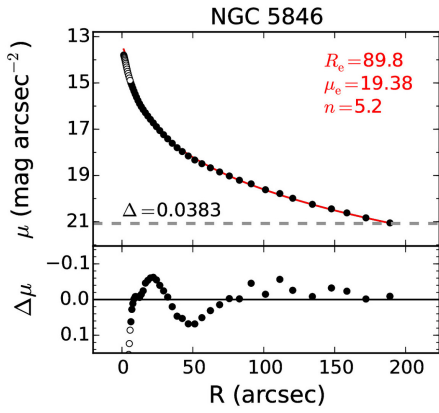


Figure 14. Sersic fit to $3.6\mu\text{m}$ surface brightness profile and residuals as a function of circular equivalent radius. The *upper* panel shows the data points (with excluded data points shown by open circles) and the best fit Sersic profile in red. Parameters for the Sersic fit are given in the top right. The dashed line shows $3\times$ the rms of the sky background level. Δ gives the rms of the residuals in mag arcsec^{-2} . The *lower* panel shows the residuals of the Sersic model fit minus the surface brightness data.

Figure 15. Sersic fit to $3.6\mu\text{m}$ surface brightness profile and residuals as a function of circular equivalent radius for non-SLUGGS galaxies. The *upper* panel shows the data points (with excluded data points shown by open circles) and the best fit Sersic profile in red. Parameters for the Sersic fit are given in the top right. The dashed line shows $3\times$ the rms of the sky background level. Δ gives the rms of the residuals in mag arcsec^{-2} . The *lower* panel shows the residuals of the Sersic model fit minus the surface brightness data.

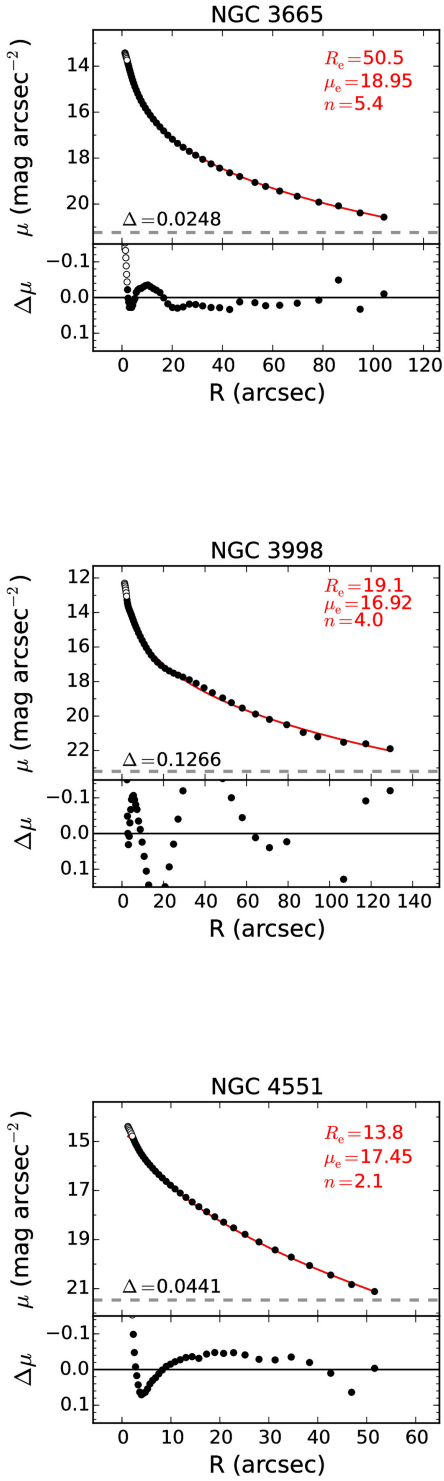


Figure 16. Sersic fit to $3.6\mu\text{m}$ surface brightness profile and residuals as a function of circular equivalent radius for non-SLUGGS galaxies. The *upper* panel shows the data points (with excluded data points shown by open circles) and the best fit Sersic profile in red. Parameters for the Sersic fit are given in the top right. The dashed line shows $3\times$ the rms of the sky background level. Δ gives the rms of the residuals in mag arcsec $^{-2}$. The *lower* panel shows the residuals of the Sersic model fit minus the surface brightness data.